Acta Biomaterialia 9 (2013) 8075–8088

Contents lists available at SciVerse ScienceDirect

Acta Biomaterialia

journal homepage: www.elsevier.com/locate/actabiomat

A self-assembling peptide reduces glial scarring, attenuates post-traumatic inflammation and promotes neurological recovery following spinal cord injury

Yang Liu [a], Hui Ye [a], Kajana Satkunendrarajah [a], Gordon S. Yao [a], Yves Bayon [b], Michael G. Fehlings [a,c,d,*]

[a] Department of Genetics and Development, Toronto Western Research Institute and Spinal Program, Krembil Neuroscience Centre, University Health Network, Toronto, Ontario, Canada
[b] Covidien – Sofradim Production, Trevoux, France
[c] Department of Surgery, University of Toronto, Ontario, Canada
[d] Institute of Medical Sciences, University of Toronto, Ontario, Canada

ARTICLE INFO

Article history:
Received 5 September 2012
Received in revised form 23 May 2013
Accepted 3 June 2013
Available online 14 June 2013

Keywords:
Spinal cord injury
Self-assembling peptide
Nanofiber
Neurological recovery

ABSTRACT

The pathophysiology of spinal cord injury (SCI) involves post-traumatic inflammation and glial scarring which interfere with repair and recovery. Self-assembling peptides (SAPs) are molecules designed for tissue engineering. Here, we tested the performance of $K_2(QL)_6K_2$ (QL6), a SAP that attenuates inflammation and glial scarring, and facilitates functional recovery. We injected QL6 into the spinal cord tissue of rats 24 h after clip compression SCI. QL6 led to a significant reduction in post-traumatic apoptosis, inflammation and astrogliosis. It also resulted in significant tissue preservation as determined by quantitative histomorphometry. Furthermore, QL6 promoted axonal preservation/regeneration, demonstrated by BDA anterograde and Fluorogold retrograde tracing. In vitro experiments found that a QL6 scaffold enhanced neuronal differentiation and suppressed astrocytic development. The electrophysiology confirmed that QL6 led to significant functional improvement of axons, including increased conduction velocity, reduced refractoriness and enhanced high-frequency conduction. These neuroanatomical and electrophysiological improvements were associated with significant neurobehavioral recovery as assessed by the Basso–Beattie–Bresnahan technique. As the first detailed examination of the pathophysiological properties of QL6 in SCI, this work reveals the therapeutic potential of SAPs, and may suggest an approach for the reconstruction of the injured spinal cord.

1. Introduction

Neurotrauma, including spinal cord injury (SCI), is a leading cause of neurological disability and death. The pathophysiology of SCI involves a primary mechanical injury followed by a series of secondary molecular and cellular changes [1]. The inherent challenge of developing therapies aimed at treating SCI is rooted in the complexity of its pathobiology, which includes invasion of inflammatory agents, ongoing apoptosis of neural cells, demyelination, formation of cavities or cysts, glial scarring and the loss of complex neural circuitry [2]. The combined presence of cavitation and glial scarring acts as a physical and chemical barrier to repair, plasticity and regeneration. Current therapeutic strategies for acute SCI are chiefly aimed at preventing tissue loss with pharmacological agents. No interventions have yet been developed to reconstruct post-traumatic cyst cavities. Hence, it is attractive to develop a tissue-engineered scaffold which could act as a bridge for endogenous cell migration, axonal elongation and plasticity.

In the past decade, self-assembling peptides (SAPs) have been developed for tissue engineering and protein delivery [3]. Synthetic SAPs can self-assemble into nanofibers in situ under physiological conditions, without apparent immune response [4]. These properties make SAPs appealing for application in SCI because they can be injected directly into the lesion site, thus minimizing the damage to the cord which can occur with the implantation of solid scaffolds. Liquid SAPs can readily fill the cavities, regardless of their size and shape, and become integrated with host tissue after self-assembling to a hydrogel. The use of SAPs is a novel approach in providing a nanofibrillar biocompatible structure, similar to the native extracellular matrix. This direct contact between nanofibers and the extracellular matrix may be critical in facilitating

* Corresponding author at: Division of Neurosurgery, Division of Genetics and Development, University Health Network, University of Toronto, 399 Bathurst St. 4WW-449, Toronto, Ontario, M5T 2S8 Canada. Tel.: +1 (416) 603 5229; fax: +1 (416) 603 5745.
E-mail address: Michael.Fehlings@uhn.on.ca (M.G. Fehlings).

1742-7061
http://dx.doi.org/10.1016/j.actbio.2013.06.001

cell–scaffold interaction [5,6]. SAP nanofiber scaffolds have become increasingly important, not only in studying the three-dimensional microenvironment, but also in developing approaches for a wide range of innovative medical technologies, including regenerative medicine [5]. It has been reported that after SCI, in vivo treatment with IKVAV containing SAP amphiphile (IKVAV PA) reduces astrogliosis and cell death and promotes regeneration of both descending motor fibers and ascending sensory fibers [7]. In this study, it was necessary to promote PA bioactivity by incorporating the neurite-promoting laminin epitope IKVAV into the molecular design of the scaffold. Another SAP substance found in the literature is RADA16-I (Ac-RADARADARADARADA-$CONH_2$), this peptide was found to bridge the injured spinal cord, elicit axon regeneration [8] and reduce the glial reaction and inflammation in surrounding brain tissue [9]. In a recent paper, a bone marrow homing peptide, RADA16-I SAP, functionalized by combining with a bioactive peptide, PFSSTKT (BMHP1), was found to induce a favorable matrix remodeling process and provide physical and trophic support to spinal cord tissue regrowth, cellular infiltration and axon regeneration/sprouting [10]. However, RADA16-I has a pH of 3–4; when applied directly onto nervous tissue, this degree of acidity may cause tissue damage. Guo et al. reported that untreated RADA16-I with low pH values could be detrimental in that they cause inflammation in the host spinal cord tissue, creating distinct gaps and cysts surrounding the implants [8]. Therefore, there are certain limitations associated with the use of RADA16-I, notably its intrinsically low pH and the resultant need for prebuffering to counteract the acidity of the SAP.

$K_2(QL)_6K_2$ (QL6) is a novel SAP introduced by Dong et al. [11] and provided by Covidien. It is important to note that QL6 self-assembles into β-sheets at neutral pH, a feature that is rare among peptides, which generally form insoluble β-sheet assemblies [11]. The present study was designed to determine the effects of QL6 in the reconstruction of the injured spinal cord when administered at the clinically relevant time point of 24 h post-SCI. We reported that, without any bioactive adjunct, QL6 can provide favorable support for neuronal growth and functional repair post-SCI, as shown by combined neuroanatomical, electrophysiological and neurobehavioral data. These observations suggest that the SAP QL6 is a promising biomaterial for central nervous system injury.

2. Materials and methods

2.1. Animal SCI and intraspinal microinjection

All animal experiments were conducted with approval from the Animal Care Committee, University Health Network (Toronto, Canada). The aneurysm clip compression/contusion model of SCI used in our laboratory has been characterized extensively and described previously [12,13]. Briefly, adult female Wistar rats (250–300 g; Charles River, Montreal, Canada) received laminectomies of mid-thoracic vertebral segments T6–T7. A modified clip calibrated to a closing force of 35 g was applied extradurally to the cord for a duration of 1 min. The animals were divided into two groups in a randomized and blinded manner, namely the QL6 treatment group and a saline control group. We chose a QL6 concentration of 1% (w/v) for gel formation that can mimic extracellular matrix [7,11]. Gelain et al. [14] reported that a SAP concentration of 1% (w/v) yielded a hydrogel scaffold stiffness similar to that of the spinal cord. The opacity and mechanical stiffness of the hydrogels increase with increasing peptide concentration. 1% (w/v) peptide concentration demonstrated a medium fiber density under scanning electron microscopy observation, which could have a stable nanostructure (unpublished data).

Using a stereotaxic frame and glass capillary needle connected to a Hamilton microsyringe, a total of 10 μl was injected into the dorsal spinal cord 24 h after SCI. Two intraspinal injections were made bilaterally rostral and caudal to the injury site starting at 2 mm below the dorsal surface and then at intervals of 0.5 mm (three sites), with 1.67 μl being injected at each interval amounting to a total dose of 5 μl at each stump (Fig. 1B). The injection rate was 0.5 μl per minute and, at the end of injection, the capillary was left in the cord for at least 1 min to allow diffusion from the injection site.

2.2. Electron microscopic characterization of the scaffolds

2.2.1. Transmission electron microscopy (TEM)

QL6 samples were applied to carbon-coated copper grids, and were allowed to adsorb for 1 min. The grids were then stained by 2% phosphotungstic acid for 30 s for negative staining. The stained grids were allowed to air dry before imaging. Electron microscopy images were obtained using a Hitachi H-7000 transmission electron microscope at an 75 kV accelerating voltage.

2.2.2. Scanning electron microscopy (SEM)

Samples were soaked in 5% glutaraldehyde at 4 °C for 2 h, slowly dehydrated in 10% increment steps of ethanol for 5 min each, and placed in a pressurized liquid CO_2 siphon for 1 h using a CO_2 critical point dryer. Scaffolds were coated with gold with a sputter coater, and images were taken with a Hitachi S-3400N scanning electron microscope.

2.3. Histological processing and tissue sparing assessment

Animals were perfused transcardially with 4% paraformaldehyde in 0.1 M phosphate-buffered saline (PBS). The tissues were then cryoprotected in 25% sucrose in PBS. A 2 cm length of the spinal cord centered at the injury site was embedded in tissue-embedding medium. The injured segment was snap frozen and sectioned on a cryostat (Leica CM3050S). Serial spinal cord sections at 500 μm intervals were stained with myelin-selective pigment luxol fast blue (LFB) and the cellular stain hematoxylin–eosin (HE) to identify the injury epicenter.

2.3.1. Assessment of tissue sparing at the injury site

Tissue sparing was analyzed 8 weeks after SCI, at the center of the lesion, 2 mm rostral and 2 mm caudal to the epicenter. Sections were stained with LFB-HE. The measurements were carried out on coded slides using ImageJ software (NIH). Cross-sectional residual tissue was normalized with respect to total cross-sectional area and the areas were calculated every 500 μm within the rostrocaudal boundaries of the injury site.

2.4. GFAP and Iba-1immunohistochemical procedures and image analysis

The following primary antibodies were used: mouse anti-glial fibrillary acidic protein (GFAP) (1:500; Chemicon International, Inc., Temecula, CA) for astrocytes, mouse anti-Iba-1 (1:500, Wako, Japan) for macrophages/microglia [15]. The sections were rinsed three times in PBS after primary antibody incubation and incubated with fluorescent Alexa 568 goat anti-mouse/rabbit secondary antibody (1:400; Invitrogen, Burlington, ON) for 1 h. The sections were rinsed three times with PBS and coverslipped with Mowiol mounting medium containing DAPI (Vector Laboratories, Inc., Burlingame, ON) to counterstain the nuclei. The images were taken using a Leica epifluorescence microscope.

For immunodensity measurements of GFAP and Iba-1, four sections were selected at the epicenter, as well as at 1 and 2 mm (two rostral and two caudal) from the injury epicenter in each animal. We photographed the entire transverse section at 10× primary

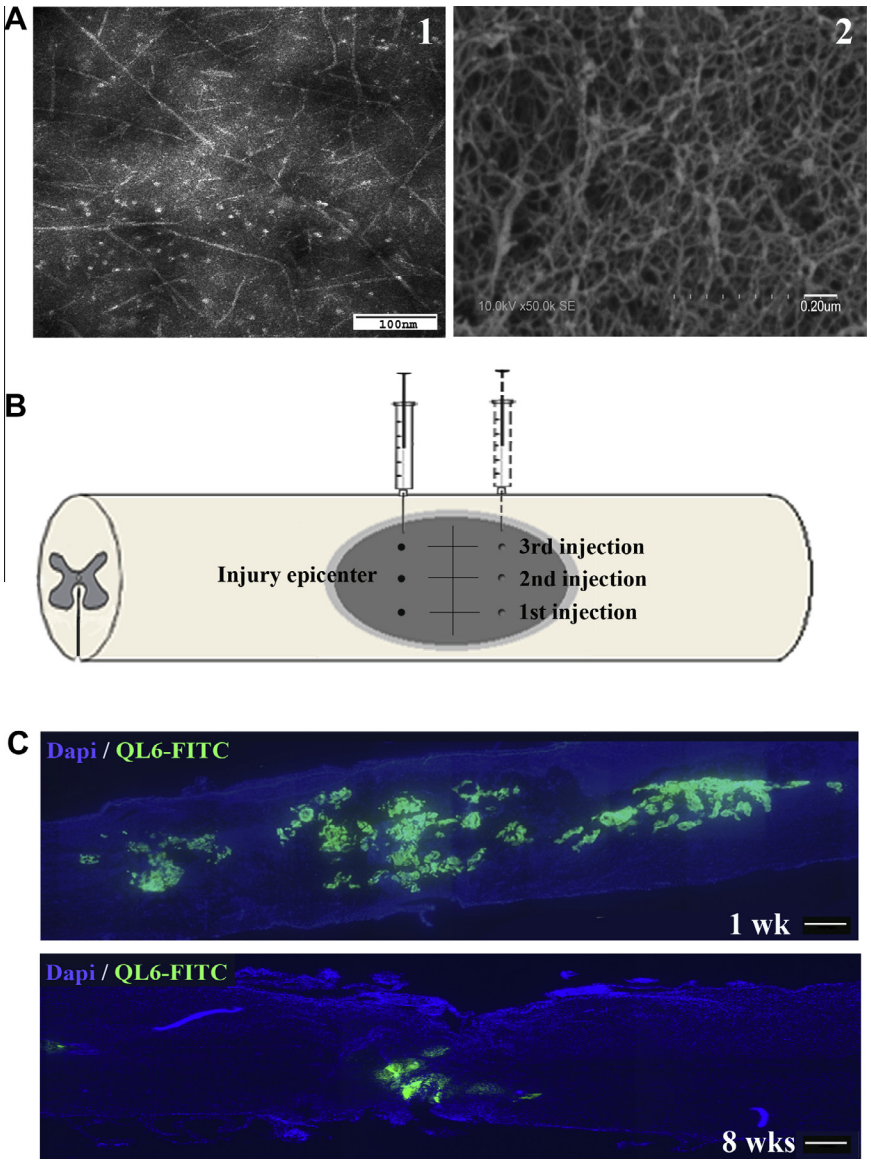

Fig. 1. Delivery of the SAP QL6 into the injured rat spinal cord. (A1) TEM image of QL6 peptide in water. Scale bar: 100 nm. (A2) SEM image of QL6 nanofiber scaffold at 1% (w/v) peptide concentration assembled in PBS solution at 2 h. Scale bar: 0.2 μm. (B) Two intraspinal injections were made bilaterally rostral and caudal to the injury site for a total dose of 10 μl. (C) Longitudinal sections of rat spinal cord obtained at the injury site 1 week and 8 weeks after compression injury and QL6-FITC injection. The QL6 was successfully injected into the cord. It aggregated in the epicenter and diffused rostrocaudally into the penumbra at 1 week, and almost biodegraded at 8 weeks. Scale bar: 600 μm.

objective using tiling and stitching software (StereoInvestigator). Each scan was performed using identical laser power, gain and offset values. The immunodensity of each image was measured using NIH ImageJ software. The relative fluorescence values were expressed as fold increases over the baseline (uninjured cord). We divided the integrated density by the sample area to calculate the mean density per unit area. This calculation was performed to compensate for the different sizes of the region of interest in the spinal cord. The final immunodensity values were then averaged for each group [16].

2.5. Apoptotic cell death and quantification

An in situ terminal-deoxy-transferase mediated dUTP nick end-labeling (TUNEL) apoptosis kit (Chemicon International, Inc., Temecula, CA) was used to label apoptotic cells as described in the manufacturer's instructions. Briefly, sections were rinsed three times in PBS and, once in equilibration buffer, followed by application of terminal deoxynucleotidyl transferase enzyme for 1 h in a humidified chamber at 37 °C. To label apoptotic cells, an anti-digoxigenin–fluorescein conjugate solution was applied to sections for 1 h at room temperature in the dark. Slides were mounted and coverslipped with Mowiol containing DAPI. Anti-cleaved caspase-3 (1:200; Cell Signaling Technology, Danvers, MA) immunohistochemistry was also used to detect and confirm apoptosis. The images of each section were taken using a Leica microscope with StereoInvestigator. The numbers of TUNEL and cleaved caspase-3-positive nuclei were counted at the epicenter, 1 and 2 mm (rostral and caudal, four sections were selected at each site) from the injury epicenter. The whole section was counted to include all apoptotic nuclei visible in each tissue section.

2.6. BDA anterograde tracing of the corticospinal tract

One week before being killed, rats underwent anterograde tracing of the corticospinal tract (CST) with biotinylated dextran amine (BDA). Under anesthesia, rats were positioned in a stereotaxic

frame. BDA (10%, 10,000 MW; Invitrogen, Burlington, ON) was injected unilaterally into the left sensorimotor cortex at eight sites (0.5 μl per site) following a previously described method [16]. Six transverse sections per animal at 2, 4 and 8 mm (2 sections per site) to the injury site were selected for immunohistochemical processing against BDA. The sections were incubated with the following reagents: 0.03% hydrogen peroxide (H_2O_2) in absolute methanol for 30 min at 4 °C, Vectastain AB (ABC Elite Kit, Vector Laboratories) in PBS containing 0.3% Triton X according to manufacturer's instructions for 2 h. Tissues were then incubated for 10 min with the NovaRED substrate kit (Vector Laboratories) for visualization of antibody binding. The slides were then dehydrated through an alcohol series, cleared in xylene and coverslipped.

We photographed the entire horizontal section at 10× primary objective using tiling and stitching software (StereoInvestigator). Using ImageJ Software (NIH), we measured the integrated density of BDA labeling in a traced area. Background intensity from an area with no BDA positive staining was subtracted from the intensity value to correct for nonspecific reactions. The density values at the BDA labeled region were normalized to the values obtained from control cord.

2.7. Fluorogold (FG) retrograde tracing and neuronal counting

Animals underwent complete spinal cord transection at the level of T10 under anesthesia, for introduction of the retrograde axonal tracer fluorogold (FG; Fluorochrome, LLC, Denver, CO) as described in a previous publication from our laboratory [17]. In brief, FG was dissolved to a final concentration of 4% (w/v) in PBS and filter-sterilized. Sterile 5 mm × 5 mm × 2 mm gel foam pledgets were immersed in the FG solution and then placed into the transection sites. One week subsequent to FG implantation, the brain was extracted after a transcardial perfusion fixation. The brains were cut on a cryostat (Leica model CM3050) in 40 μm coronal sections, from the caudal extent of the medulla to the rostral extent of the third ventricle. Identification of target regions, i.e. red nucleus and vestibular nuclei, was performed under Zeiss 510 laser confocal microscope.

To assess numbers of neurons labeled by retrograde tracing, every fifth section of the embedded brainstem was identified according to the rat brain atlas of Paxinos and Watson (1998). The total number of FG-labeled neurons was calculated for each region according to the following formula: (rostral to caudal length of region in μm/40 μm) × labeled neuron sum/number of sections analyzed for the region, to obtain the final summed number of labeled neurons for each region in each animal. For these profile counts, the Abercrombie formula [18] was applied to correct for overcounting.

2.8. Adult neural precursor cell (NPC) seeding on QL6 and cell differentiation assay

NPCs were harvested from the subventricular zone of adult C57BL/6 mice using a previously described method [19]. Primary neurospheres were present approximately 7 days after initial isolation and passaged weekly by mechanical dissociation and were seeded into serum-free medium containing epidermal and fibroblast growth factors. For the in vitro analysis of cell differentiation, neurospheres were differentiated by removing growth factors from media and adding 1% fetal bovine serum (FBS). The QL6 peptide was diluted with sterile distilled water, and mixed in a 1:1 volume ratio with 8% glucose in order to cope with the cellular osmolarity. QL6 SAP was assembled by adding basal medium 2 h before seeding cells. We coated a multichamber slide with matrigel (BD Biosciences, Mississauga, ON) to serve as a control. 2×10^4 cells per well were plated on the top surface of 1% QL6 SAP or matrigel.

The cultures were then grown for 7 days, at which time they were fixed with 4% paraformaldehyde. The cells were blocked and double labeled with the following primary antibodies: mouse against βIII-tubulin (1:500, Covance, Princeton, NJ) for neurons, rabbit anti-GFAP (1:500; Chemicon) for astrocytes. Alexa 488 goat anti-mouse and 568 goat anti-rabbit (1:400; Invitrogen) secondary antibodies were used to probe the primary antibodies. The images were taken using a Zeiss 510 laser confocal microscope.

2.9. In vivo electrophysiology

Motor-evoked potential (MEPs) recording: MEPs were recorded in vivo to assess the physiological integrity of spinal cord. This approach has been extensively used in our laboratory in rodent models of SCI. In vivo recordings of MEPs were recorded from the injured rats that had received QL6 treatment and compared to recordings from a group of injured control rats at 8 weeks post-injury (n = 6 per group). For MEPs, rats were under light isofluorane anesthesia (<1%), and recordings were obtained from hindlimb biceps femoris muscle. A pair of stainless steel subdermal needle electrodes was inserted into the muscle. Recordings were acquired using Keypoint Portable (Dantec Biomed, Denmark). A ground electrode was placed under the skin between the recording and stimulating electrodes. A 2 mA square pulse stimulation of 0.1 ms at a rate of 0.13 Hz was applied to the midline of the cervical spinal cord. The amplitude was determined by the difference between the positive peak and negative peak. The latency was calculated as the time from the start of the stimulus artifact to the first prominent peak. For individual rats, the mean peak amplitude and latency was measured from the averaged traces from 200 sweeps.

2.10. In vitro electrophysiology

The dissection procedures were generally similar to those described in earlier publications from our laboratory [17,19–21]. The animals were anesthetized, and the spine from the upper cervical to lower lumbar levels was quickly removed, and the spinal cord extruded by applying pressurized ice-cold artificial cerebrospinal fluid (ACSF) to the rostral end of the vertebral canal via a tightly fitting pipette tip connected to a syringe. The subsequent dissection, performed in oxygenated ice-cold ACSF, included removing the meninges and spinal roots (if left after extrusion), longitudinal hemisection of the cord and dissection of dorsal, as well as lateral and ventral white matter. The dorsal white matter strips were incubated in oxygenated ACSF for at least 1 h before recording.

Suction electrodes were applied to record compound action potentials (CAPs) from the spinal cord white matter [22]. This technique provides an excellent seal, and a stable resistance, both of which are essential to achieve consistent CAP recordings with suction techniques [23]. A bipolar electrode, made of polyimide-insulated stainless steel wires (outside diameter 0.125 mm, Plastics One, Roanoka, VA), was used for stimulation of the dorsal column. The stimulation and recording sites were approximately 5 mm apart. The stimulating pulse current (0.1 ms in duration) was applied at 15 s intervals from the SIU-PSIV6 stimulus isolation unit of a Grass S88 stimulator. The recording electrodes were connected to the head stage of an Axoprobe 1A amplifier (Axon Instruments) via an Ag/AgCl electrode. The signals were amplified 100× in DC mode (10× by Axoprobe 1A and then 10× by a custom-made DC preamplifier), processed using Digidata 1200, stored on a PC and analyzed using pClamp 10 software (Axon Instruments/Molecular Devices, USA).

CAP recordings were analyzed according to their baseline-to-peak amplitude, width, refractory period with pair pulse stimulation. The maximal amplitude of the CAPs was recorded at supra-

threshold stimulation intensity. The refractoriness of the axons was examined by stimulating the cord by pair pulses with different intervals (starting from 0.5 ms with an increment of 0.5 ms), and by examining the recovery of the second CAP in comparison to the first one. To examine the ability of spinal cord axons to conduct signals at high frequency, the cord was stimulated with 20, 50 and 100 Hz (100 pulses in total), respectively. The amplitude of the last CAP was expressed as a percentage of the first CAP in the train, a method used previously by our laboratory [24] to estimate the fatigue of the axons induced by high-frequency stimulation (HFS).

2.11. Neurobehavioral testing

BBB open-field locomotor score: locomotor recovery of the animals was assessed by two independent observers using the 21-point Basso, Beattie and Bresnahan (BBB) open-field locomotor score [25] from 1 to 8 weeks after SCI. The BBB scale was used to assess hindlimb locomotor recovery including joint movements, stepping ability, coordination and trunk stability. Testing was done every week on a blinded basis and the duration of each session was 4 min per rat. Scores were averaged across both the right and left hindlimbs to arrive at a final motor recovery score for each week of testing.

2.12. Statistical analysis

Data were analyzed with SigmaStat (Systat Software). For comparison of groups over time (BBB behavioral testing) or distance (tissue sparing), we used two-way analysis of variance (ANOVA) with repeated measures, followed by the post hoc Bonferroni test. For neuroanatomical studies, statistical analyses of intensity measurements and cell counts were tested by Student's *t* tests where two groups were compared.

3. Results

3.1. Biodistribution and biodegradation of QL6 in injured spinal cord

To visualize the structure of the self-assembled QL6 nanofibers, we dissolved QL6 in Milli-Q water or PBS. Since the gelation of SAP is initiated by salt concentration, QL6 should not be combined with salt-containing buffers until gelation is desired. TEM was used to show the morphology of QL6 dissolved in water, the structure of a single molecule indicated that the peptide is not contaminated by other ions. When QL6 was dissolved in PBS and was allowed to assemble for 2 h, SEM demonstrated the network scaffold of QL6 nanofiber (Fig. 1A).

One advantage of SAPs is their ability to self-assemble into nanofibers when injected into tissue. To evaluate the delivery and biodistribution of the QL6 in vivo, at 24 h after SCI, the lesion site was injected with a fluorescent derivative of the QL6 (QL6-FITC was mixed in a 1:9 volume ratio with QL6), and the rats were killed at 1, 4, 6 and 8 weeks after injection. Images taken from 1 week after injection show excellent distribution of the QL6 scaffold in the injured cord, particularly rostrocaudally into the perilesional "penumbra" zone, where we observed that QL6 diffused for approximately 1 cm centered on the injury epicenter with our injection method (Fig. 1B). The QL6 scaffold degraded gradually over time. At 8 weeks post-injection, although QL6 fluorescent is still present, most has biodegraded (Fig. 1C).

3.2. QL6 reduces astrogliosis and inflammation

One of the major obstacles to neuronal regeneration after SCI is glial scarring that occurs in part as a result of reactive astrogliosis, which has been suggested to be involved in neurotoxicity and inflammation [26]. We examined whether the QL6 affected the population of reactive astrocytes and inflammation around the SCI lesion. Cellular hypertrophy and increases in GFAP are the hallmarks of astrocyte reactivity and occur after SCI. Using immunohistochemical analyses, we examined the expression of GFAP and Iba1 as markers for reactive astrocytes and macrophages/microglia, respectively. We focused on the lesional and perilesional areas. At 1 week after SCI, GFAP and Iba1 immunohistochemistry revealed no apparent difference between the injected control and QL6-injected groups. Eight weeks post-SCI, interestingly, there were obvious reductions in astrogliosis and inflammation in the QL6-treated animals (Fig. 2A, B). GFAP staining revealed a significant reduction in astrogliosis in the QL6-treated group in the lesion area (1.30 ± 0.17 for QL6; 2.58 ± 0.33 for control; $P < 0.01$) and in perilesional areas (1 mm: 2.56 ± 0.18 for QL6; 3.15 ± 0.13 for control; $P < 0.05$) (Fig. 2C). Similarly, Iba1 immunointensity revealed a significant reduction of inflammation in the QL6-injected group (control: 3.9 ± 0.24 vs. QL6: 2.95 ± 0.23) at the lesioned areas ($P < 0.05$) (Fig. 2D).

3.3. QL6 attenuates post-traumatic apoptosis

Previous studies from our group have shown that apoptotic cell death occurs as early as 6 h following SCI, peaks at 7 days and is still evident at 14 days post-injury [27]. To determine the effects of QL6 treatment on apoptotic cell death we used two marks of apoptosis. TUNEL and activated caspase-3 immunostaining was performed 1 week after injury. TUNEL- and caspase-3-positive cells were found throughout the gray and white matter in the injured spinal cord, with the greatest concentration close to the lesion site, and a gradual decrease away from the epicenter. As shown in Fig. 3, QL6 treatment was associated with a significant reduction in counts of TUNEL-positive cells at epicenter and on either side of the lesion epicenter. Cleaved caspase-3 immunohistochemistry revealed a similar result to TUNEL counts, but there was no significant difference between the two groups at 2 mm away from the epicenter by caspase-3 quantification. The mean ± SEM numbers of apoptotic cells derived from control vs. QL6 injected animals were: TUNEL: 127 ± 8.5 vs. 75 ± 8.7, caspase-3: 113 ± 5.6 vs. 74 ± 9.1 (epicenter); TUNEL: 100 ± 6.1 vs. 55 ± 6.7, caspase-3: 80 ± 7.1 vs. 59 ± 6.0 (1 mm) and TUNEL: 85 ± 5.2 vs. 52 ± 3.8, caspase3: 66 ± 6.3 vs. 56 ± 4.2 (2 mm), respectively.

3.4. QL6 enhances tissue preservation at the lesion site

Eight weeks after SCI, spinal cord cross-sections were stained serially with LFB-HE. Spinal cords from QL6-treated rats exhibited a greater extent of spared tissue when compared to tissue sections from the same location in the injured control rats (Fig. 4A). Measurements of residual tissue taken from cross-sectional areas were expressed as a percentage of the total cross-section area. A comparison of the percentages of normalized residual tissue, which is represented in Fig. 4B, was performed by two-way ANOVA with the two factors being treatment and distance from the injury epicenter. This experiment revealed an overall significant improvement in tissue preservation in the QL6-treated group ($P < 0.05$). The percentage of remaining tissue was $74.74 \pm 4.12\%$ in QL6-injected animals and $61.05 \pm 2.51\%$ in control rats at 0.5 mm rostral to the epicenter ($P < 0.01$). There was also a significant increase in the preserved neural tissue at 1 mm rostral to the epicenter ($82.93 \pm 4.63\%$ in the QL6-treated group vs. $70.63 \pm 4.32\%$ in the control group; $P < 0.05$). However, there was no marked difference observed in tissue preservation in the caudal region between two groups. This could be due to different vascular injury and recovery at rostral vs. caudal regions in our SCI model.

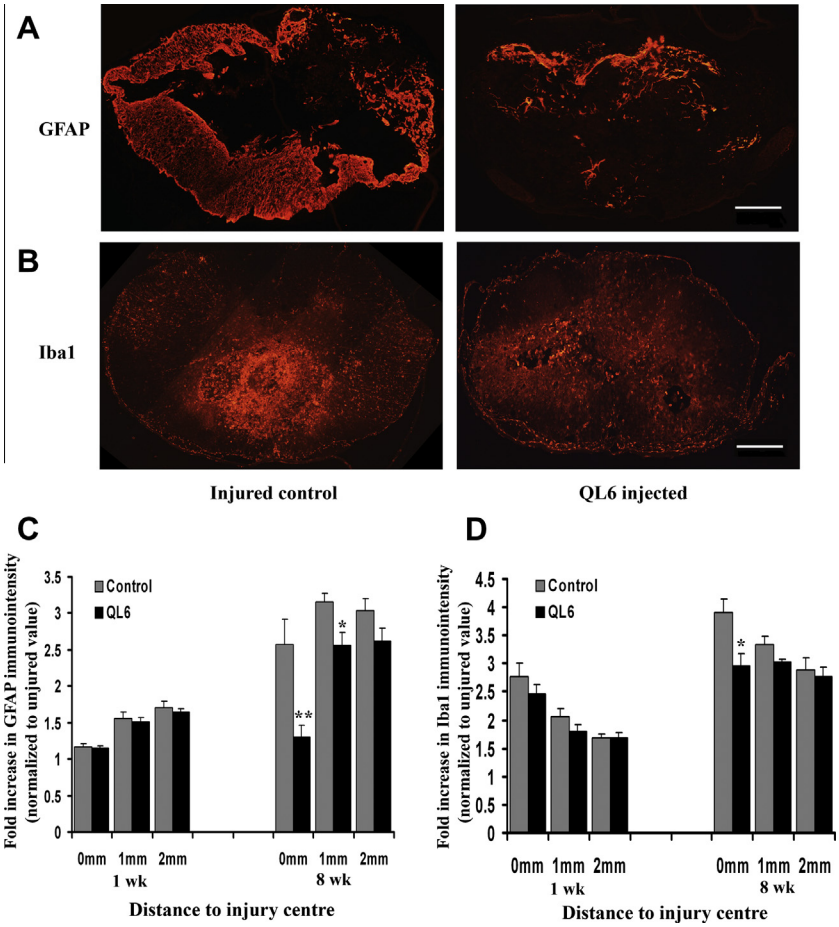

Fig. 2. QL6 leads to reduced astrogliosis and inflammation in chronic SCI. Photomicrographs showing a transverse section of rat spinal cord stained with GFAP (A) and Iba1 (B) in control and QL6-injected animal. There is less astrogliosis and inflammation in the QL6-injected animals. Scale bar: 250 μm for (A) and (B). 8 weeks after SCI, GFAP (C) and Iba1 (D) immunofluorescence levels in the QL6-injected animals are significantly reduced compared with control animals. Data are mean ± SEM (bars) values, $n = 6$ per group; $^{**}P < 0.01$, $^{*}P < 0.05$. Images were taken from the injury epicenter.

3.5. QL6 promotes CST axonal preservation and leads to increased counts of neurons retrogradely labeled by fluorogold

The corticospinal tract (CST) consists of axons from pyramidal neurons originating in the motor cortex extending to the contralateral spinal cord. It represents the primary transmission tract for brain-controlled voluntary movement. To investigate whether the SAP QL6 could promote axonal sparing in the chronically injured spinal cord, we examined the plasticity of CST collaterals innervating the spinal cord using anterograde BDA labeling. Notably, we observed an increase in BDA-labeled fibers in the dorsal funiculus of the contralateral spinal cord in the QL6-injected group compared with the control group (Fig. 5A). Quantitative analysis of the BDA tracing regions revealed a significant increase in the density of BDA-labeled collaterals in the QL6-injected rats when compared to the injured controls at all distances (ranging from 2 to 8 mm) rostral to the lesion with the highest value detected at 4 mm (a 1.63-fold increase) (Fig. 5B). However, no evidence of long-distance CST axon preservation/regeneration at and beyond the lesion was detected (data not shown).

The survival of axons traversing the injury site was also assessed by counting the FG-labeled neurons in brainstem nuclei following spinal cord transection and FG impregnation distal (T10) to the injury site. Counts of retrogradely labeled neurons were performed in the red nucleus, vestibular nuclei and the total brainstem (which includes red nucleus, vestibular nuclei, raphe nuclei and reticular formation). Representative sections of FG-labeled neurons in the red nucleus from animals treated with saline and QL6 are shown in Fig. 5C. QL6-injected animals showed higher overall neuronal counts in the red nucleus, vestibular nuclei and total brainstem (Fig. 5D). The number of labeled neurons was significantly higher in the red nuclei (665.38 ± 51 for control vs. 856.27 ± 42 for QL6; $P < 0.05$) and total brainstem (4830.15 ± 498 for control vs. 6767.80 ± 422 for QL6; $P < 0.05$) in the QL6-injected group. The numbers of labeled neurons from QL6-injected animals in the vestibular nuclei (545.13 ± 57 for control vs. 768.45 ± 96 for QL6; $P = 0.09$) was not significantly different from those in saline-treated controls.

3.6. Evaluation of NPC differentiation within the QL6 SAP scaffolds

We have shown convincing data that illustrate the ability of QL6 scaffold to inhibit astrogliosis while markedly enhancing axonal density. After SCI, neurogenesis is largely mediated by endogenous stem cell differentiation, which produces several cell types including neurons and glia. To further understand the differential capability of QL6 in promoting neuronal and astroglial growth, we examined the effects of QL6 on the differentiation capability of NPCs into neurons and astroglial, respectively. As shown by immunocytochemistry (Fig. 6A), the QL6 nanofiber scaffold promoted greater differentiation of the NPCs into neurons, and suppressed astrocytic differentiation when compared with the matrigel control. In agreement with our previous study [19], we found that when cultured on matrigel with 1% FBS, neurons represented

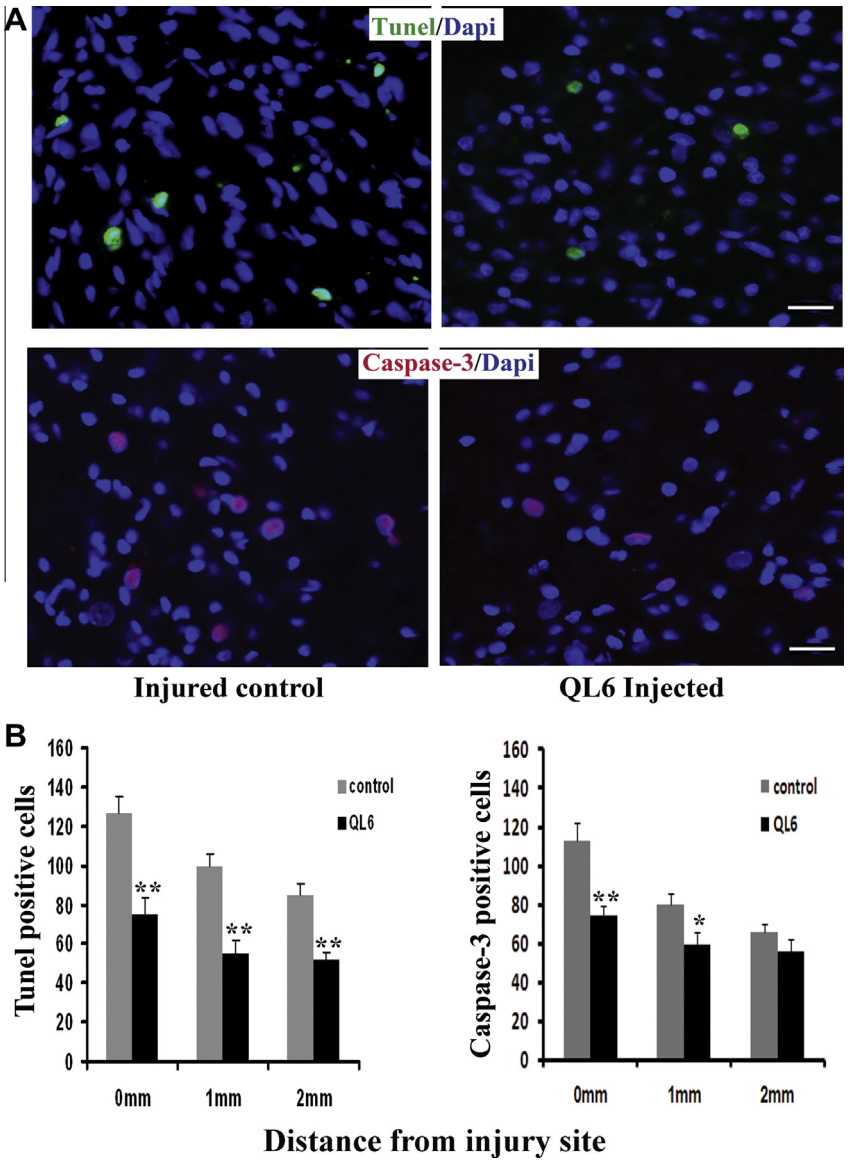

Fig. 3. QL6 administration reduced post-traumatic apoptosis after SCI. (A) Representative sections from a QL6-injected and control animal respectively immunostained with TUNEL and cleaved caspase-3 at 1 week after SCI. Section stained with TUNEL in green, caspase-3 in red and nuclear marker DAPI in blue; scale 40 μm. A reduction of TUNEL- and caspase-3-positive cells was observed in the QL6-injected group. (B) Bar graph showing that there was a significant decrease in TUNEL- and caspase-3-positive cell death in the QL6 treatment group vs. control group Values are mean ± SEM, $n = 6$ per group; $^{**}P < 0.01$; $^{*}P < 0.05$.

6 ± 0.6% of differentiated NPCs as indicated by their expression of the neuronal marker βIII-tubulin, while astrocyte lineage cells were the major cell type observed with 64 ± 2.2% of the cells staining positively for GFAP because serum composition favors astrocyte specification. In contrast, there were about 14 ± 0.9% of total cells staining positive for βIII-tubulin and 33 ± 1.6% astrocyte differentiation cultured on QL6 nanofiber network for 7 days (Fig. 6B). Inhibition of astrocyte proliferation is believed to be important in the prevention of the glial scar, a known barrier to axon elongation.

3.7. QL6 treatment enhances MEPs

After QL6 injection, we observed increased axon preservation. These studies suggested that the conduction capability of the spinal axons could be improved in the treatment group. To test this hypothesis, we recorded MEPs from both injured control and QL6-injected groups. At 8 weeks post-SCI both the treated and control groups of rats displayed a biphasic deflection pattern. QL6-treated animals had significantly higher peak amplitude compared to the injured control animals. The peak amplitude of the QL6-treated animals was 5.46 ± 1.29 μV while the control rats had an amplitude of 1.79 ± 0.41 μV ($P < 0.05$). Latency was also shorter in the treated group compared to control animals, indicating a faster conduction velocity in the QL6 group. The peak latency of the control group was 25.97 ± 2.12 ms while the QL6-treated animals had a significantly shorter latency of 20.03 ± 1.48 ms ($P < 0.05$) (Fig. 7).

3.8. QL6 treatment enhances the electrophysiological properties of dorsal column axons in isolated ex vivo recordings

CAP recording from the dorsal column of the spinal cord provides a further readout of functional recovery after QL6 treatment. We first characterized the amplitude of the CAPs, since CAP amplitude is directly associated with the number of axons available to carry nerve pulses. The axonal conduction properties were exam-

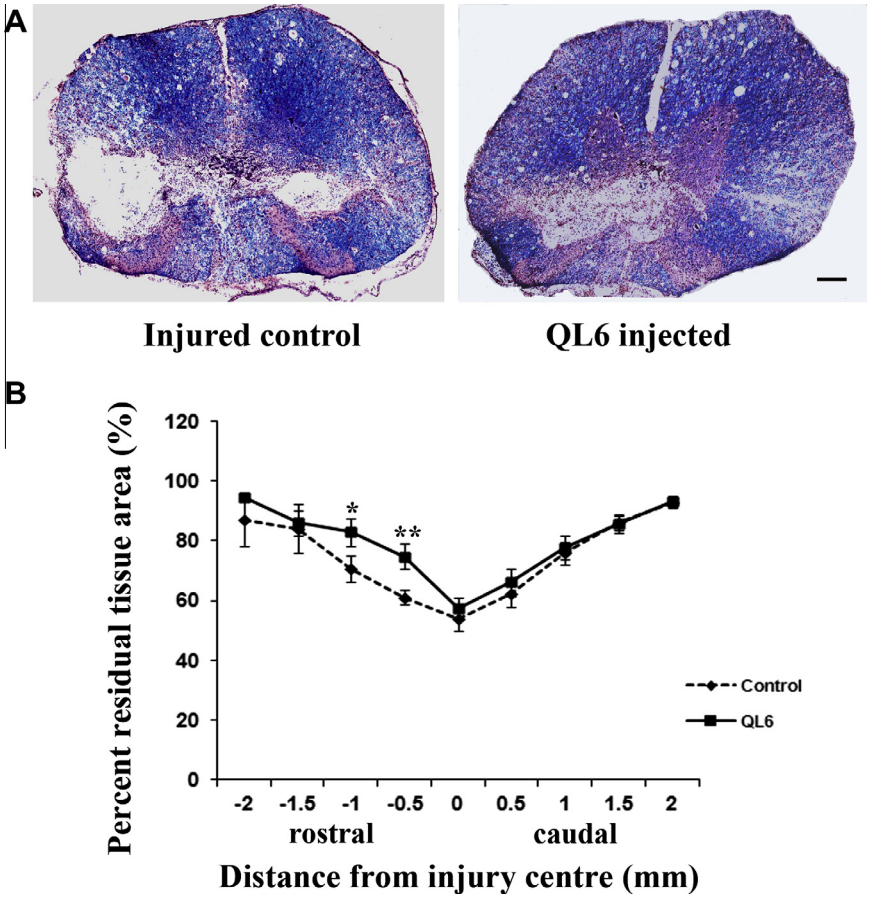

Fig. 4. QL6 improves spinal cord tissue preservation. (A) Representative sections taken 0.5 mm rostral to the epicenter from a QL6-treated and saline control animal respectively stained with LFB and HE (scale bar: 300 μm) 8 weeks after SCI. QL6-treated spinal cord exhibited a larger extent of spared tissue than control animal tissue. (B) Per cent normalized residual tissue in QL6 treatment (■) vs. control (♦) group. There was a significant different between QL6-treated animals vs. controls by two-way ANOVA with post hoc (Bonferroni) test. $^{*}P < 0.05$ and $^{**}P < 0.01$: significantly increased tissue area in QL6-treated animals at different distances from injured epicenter. Data are mean ± SEM (bars) values ($n = 10$ per group).

ined using low-frequency stimulation (1 pulse every 15 s) with suprathreshold stimulus. We found that the CAP amplitude was significantly larger in the QL6-treated cords than in the injured cords (3.23 ± 0.82 mV vs. 0.97 ± 0.03 mV; $P < 0.05$—see Fig. 8A).

Previous studies have reported that the refractory period of axons is increased after SCI [24]. Here, we investigated whether QL6 injection can alleviate axonal refractoriness after SCI. To assess the refractoriness of the spinal cord, paired stimuli with varied intervals were delivered to the cord, and we measure the minimum time intervals for the second pulse to trigger CAP (absolute refractory period), as well as the full recovery of the CAPs (relative refractory period). Varying the intervals between the two paired pulses successfully yielded a clear estimation of the absolute refractory periods. We observed a significant decrease ($P < 0.01$) in the absolute refractory period in the QL6-treated groups in comparison to the injured control (Fig. 8B). Similarly, QL6-treated cords also exhibited a decreased relative refractory period (Fig. 8C). Taken together, these data indicate that QL6 treatment significantly reduces axonal refractoriness in injured cords.

3.9. QL6 treatment improves high-frequency conduction

Previous studies have shown that axonal responses to high-frequency signals were compromised after SCI [24]. Hence, we tested if QL6 injection could rescue impaired HFS responses in the chronic SCI. We stimulated the cords with trains of repetitive stimuli composed of frequencies of 20, 50 and 100 Hz (100 pulses in total). Similar to previous publications [24,28], quantification analysis of frequency response was performed by analyzing the "fatigue ratio" of the axons, which was expressed as the ratio between the amplitude of the 100th CAP in the train as a percentage of the first amplitude of the first CAP. A higher ratio suggested a better axonal response to high-frequency stimulation. Fig. 9A shows an example of CAP changes in responses to 100 Hz stimulation in the injured cord, and in injured cord treated with QL6. Fig. 9B plots the amplitude of the CAP correspondence to the 100 Hz stimulus. QL6 injection prevented the dramatic decrease in the CAPs that was otherwise observed in the injured cords.

We also attempted other stimulation frequencies, including 20 Hz and 50 Hz. In accordance with previous studies [21], the CAP_{100}/CAP_1 ratio decreased in the injured cords in response to increased stimulation frequencies ($P < 0.001$). Overall, after QL6 injection, the injured cords were associated with a much higher CAP_{100}/CAP_1 ratio compared to those of the control injured cords ($P < 0.001$, two-way ANOVA), and this difference reached statistical significance at 20 Hz (73.8 ± 4.7 in injured cords vs. 93.5 + 2.3% in QL6-treated cords; $P < 0.01$), 50 Hz (67.2 + 2.0% in injured cords vs. 86.1 ± 1.9% in QL6-treated cords; $P < 0.001$) and 100 Hz (51.1 + 2.5% in injured cords vs. 81.7 + 1.5% in QL6-treated cords; $P < 0.001$). Combined, these results suggest that the QL6 injection reduced the "fatigue ratio" in the injured spinal axons, and improved the high-frequency conduction of the axons.

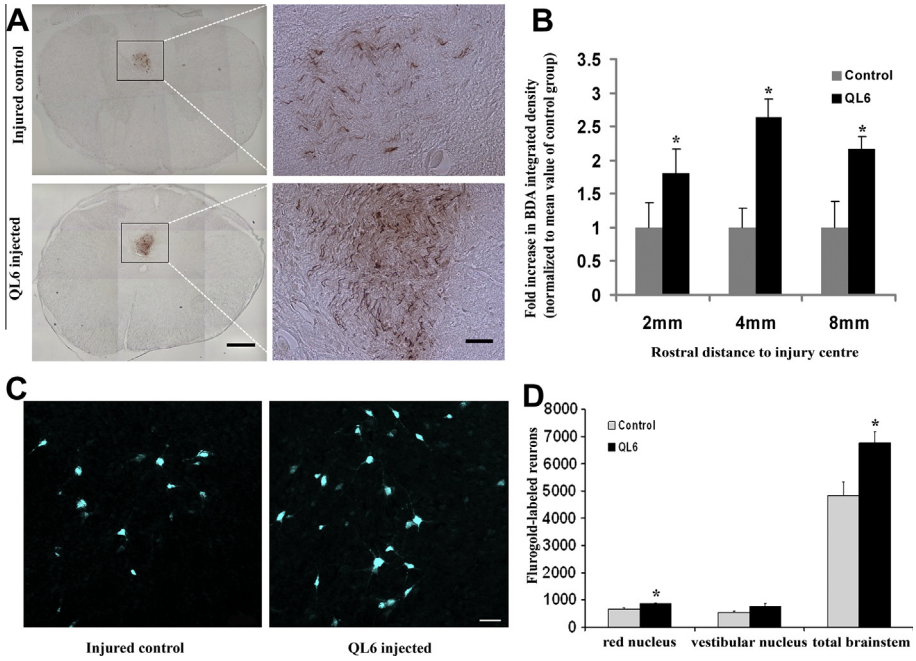

Fig. 5. QL6 promotes axonal preservation by BDA anterograde (A, B) and FG retrograde (C, D) tracing. (A) Representative sections from a QL6-injected and control animal BDA-labeled CST. Images in the right panels (scale bar: 50 μm) show the enlarged boxes in the left panels (scale bar: 300 μm). (B) 8 weeks after SCI, analysis revealed a significant increase in the density of BDA-labeled fibers in the QL6 treatment group when compared to the injured control group at 2, 4 and 8 mm rostral to the lesion center. (C) Fluorescent photomicrographs of FG-labeled neurons in the red nucleus in animals treated with either QL6 or saline. (D) There were significantly higher numbers of neurons in the red nucleus and brainstem nuclei in QL6-treated animals. Scale bar: 40 μm. Data are mean ± SEM values, $n = 6$ per group; $^{*}P < 0.05$.

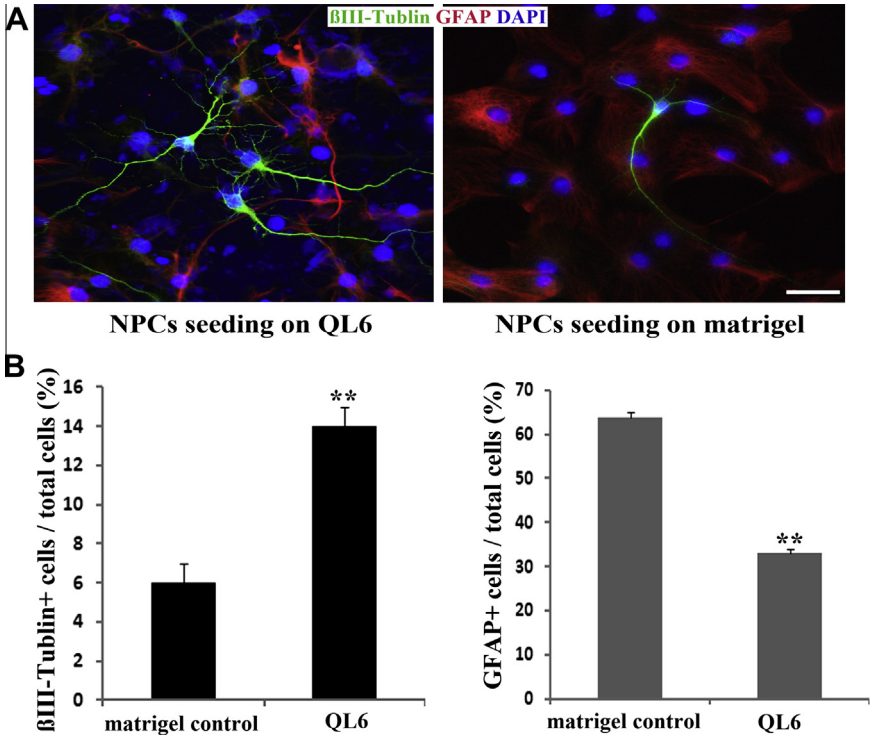

Fig. 6. Immunocytochemistry of NPCs cultured for 7 days in vitro on QL6 peptide scaffold or matrigel. (A) Differentiated neurons were labeled for βIII-tubulin (green), and differentiated astrocytes were labeled for GFAP (red). All cells were DAPI stained (cell nuclei in blue). The QL6 SAP displayed the capability to support differentiation of neurons while suppressing astrocyte differentiation compared to the matrigel control. (B) Percentage of total cells that differentiated into neurons and astrocytes. QL6 gave significantly higher percentages of differentiated neurons and lower percentages of differentiated astrocytes than those obtained with matrigel. Scale bar: 30 μm. Data are mean ± SEM values; $^{**}P < 0.001$.

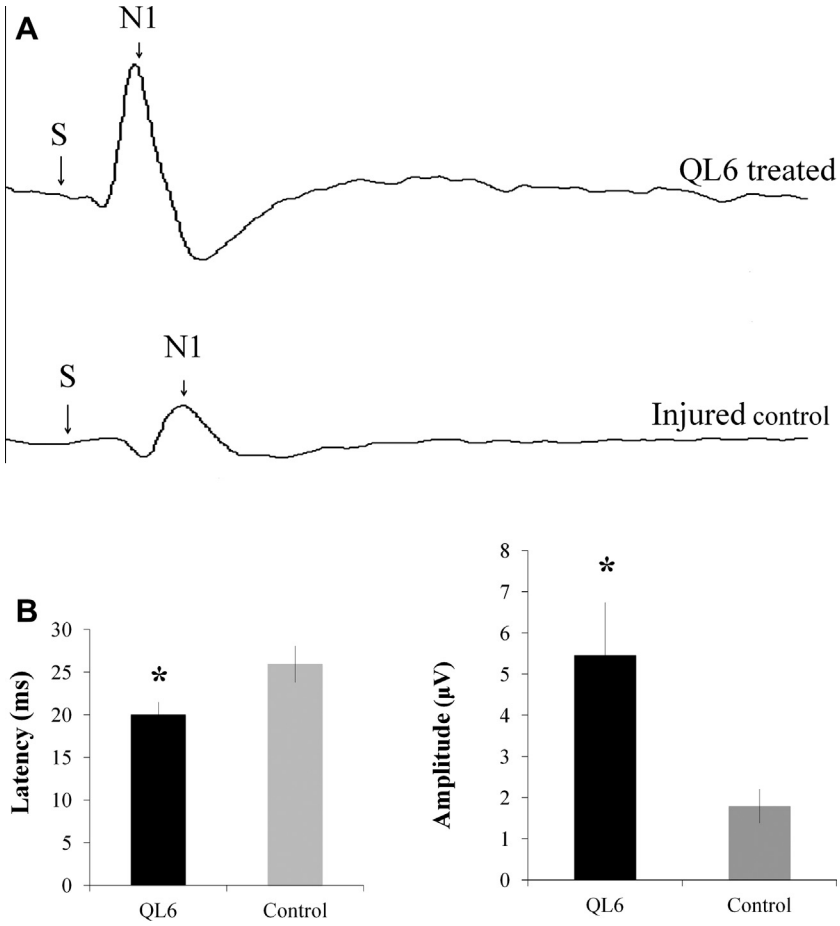

Fig. 7. At 8 weeks post-SCI, QL6 treatment resulted in significantly higher peak amplitude and shorter latency, indicating a greater preservation of motor function. (A) Representative MEP tracings from hindlimb muscle of QL6-treated animal and injured control animal where S denotes the stimulus artifact and N1 indicates the first prominent negative peak. (B) Quantitative analysis of peak latency and amplitude. The MEP amplitude was larger in QL6-treated animals compared to injured control rats. MEP latency was shorter in QL6 rats compared to injured control rats. Data are mean ± SEM values, $n = 6$ per group; $^{*}P < 0.05$.

3.10. QL6 promotes functional neurobehavioral recovery after SCI

To examine the functional effects of injecting SAP QL6 after SCI, neurobehavioral function was assessed weekly by two blinded observers using the BBB locomotor rating scale. Acutely, the hind limbs of experimental animals were completely paralyzed after SCI. Hind-limb performance gradually improved in both experimental groups. The mean BBB scores (Fig. 10) of QL6-injected animals were higher than those of saline-treated controls at every week. Using two-way repeated measures ANOVA, we found an overall significant improvement on BBB scores in the QL6-treated group ($P = 0.03$). At 6 weeks, the saline control rats reached an average score of 6, indicating non-functional movement of the three hind-limb joints without coordinated sweeping of their hind legs. In contrast, the QL6-treated rats reached an average score of 8, indicating the ability to make sweeping movements with their hind legs or coordinated plantar placement of the hind limbs without weight support. There was little further relative improvement in both experimental groups at weeks 7 and 8, suggesting a plateau in neurological recovery had been reached at week 6.

4. Discussion

The present study shows that SAP QL6 injection leads to decreased apoptosis, inflammation and glial scarring, and enhanced tissue preservation at the site of injury. QL6 improved axonal conduction as indicated by increased peak amplitude and decreased peak latency. QL6 also increased high-frequency conduction and reduced the refractoriness in the injured cords. This was manifested by significant improvement in locomotor function on the BBB scale. Taken together, these data suggest that SAP QL6 is an attractive therapeutic strategy for SCI as it preserves axons, translating to better functional outcomes. Our data demonstrated that the SAP QL6 is a prospective biomaterial for the reconstruction of the injured spinal cord.

4.1. Biocompatibility of QL6

The use of a nanofiber scaffold is a novel approach in providing extracellular matrix-like structures that are potentially conducive to cellular infiltration, proliferation, tissue repair and regeneration [29]. The QL6 peptides are characterized by periodic repeats of alternating ionic hydrophilic and hydrophobic amino acids (glutamine and leucine, respectively). QL6 shows a very strong β-sheet conformation and a population of nanofibers with uniform diameter (6 ± 1 nm) and controlled length (120 ± 30 nm). The maximum QL6 fiber lengths have not changed substantially but the average lengths increased slightly, owing to the disappearance of shorter fibers 3 weeks after assembling. Other methods, including circular dichroism and Fourier transform infrared spectrometry, did not reveal any significant changes over time [11]. Therefore, QL6 structure could be relatively stable in vitro after assembling. After injection as a liquid, QL6 demonstrated the ability to mimic the exctracellular matrix and became conducive to tissue repair/regen-

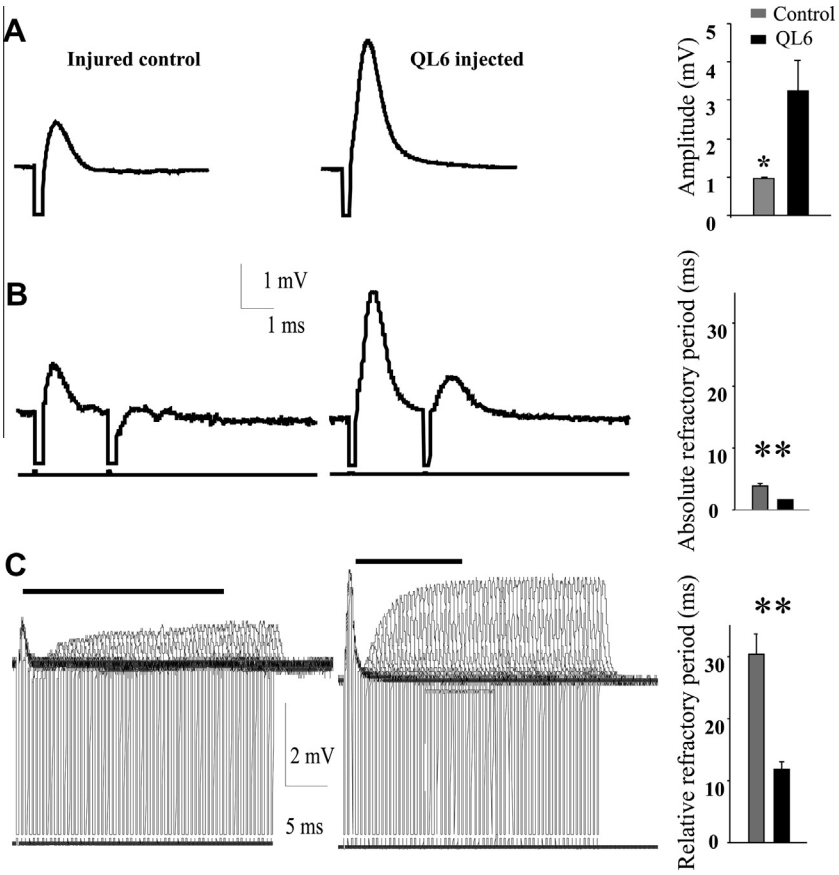

Fig. 8. Ex vivo electrophysiology. CAP recordings were performed 8 weeks after SCI. (A) QL6-treated cord is associated with a greater amplitude in CAP. (B) QL6 injection reduced the absolute refractory period in the injured cords. (C) QL6 injection reduced the relative refractory period in the injured cords. Pair-pulse protocol with different intervals was used to detect the absolute refractory period (B) and relative refractory period (C) in the injured cords and in QL6-treated cords. Note (C) depicts the overlapped traces with increment stimulating intervals. Data are mean ± SEM values, $n = 6$ per group; $^{**}P < 0.01$.

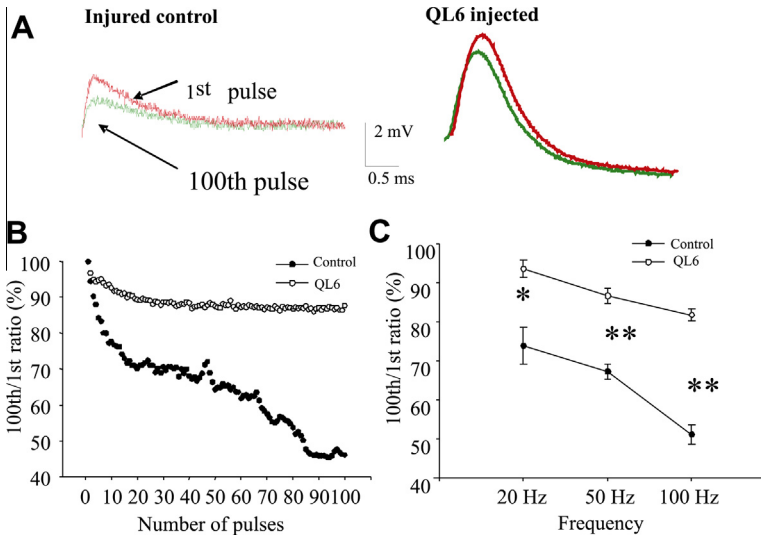

Fig. 9. Effects of QL6 treatment on axonal responses to high-frequency stimulation 8 weeks after SCI. The cords were stimulated with trains of 100 stimuli (0.1 ms in width) at varying frequencies (20, 50, 100 Hz). (A) CAPs evoked by a train of stimulus (100 Hz) in an injured cord and in a QL6-treated cord. Shown here are the 1st response and the 100th response. (B) Percentage changes in the amplitude of CAPs as a function of the number of pulses in an injured control cord and in a QL6-treated injured cord. (C) Frequency dependency of CAPs in injured cords and in QL6-treated injured cords at 20, 50 and 100 Hz, respectively. Note that injury-induced deficits in the high-frequency conduction were partially prevented with QL6 treatment ($P < 0.001$). $^{*}P < 0.01$; $^{**}P < 0.001$.

eration. Previous studies have shown that certain types of SAP, such as peptide amphiphile (PA), alone were not sufficient in neurite sprouting and differentiation [30]. It was necessary to promote PA bioactivity by incorporating the neurite-promoting laminin epitope IKVAV into the molecular design of the scaffold [7]. This study shows that the structure of QL6 itself, without any pharmacologi-

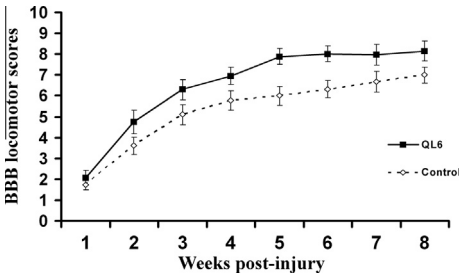

Fig. 10. The graph depicts functional hind-limb recovery over time after SCI. Injection with QL6 resulted in improved BBB scores vs. controls at week 1 through week 8. Two-way ANOVA confirmed a significant ($P = 0.03$) difference between the two groups. Data are mean ± SEM values, $n = 23$ per group.

cal adjunct, can support the functional repair of SCI, a consequence that might be related to QL6's direct action in attenuating glial scarring and post-traumatic inflammation. It is interesting to note that the soluble form of QL6 has a pH value of 7, which is able to acclimatize to the microenvironment of the host and may be more suitable for the cell entrapment and growth. The physiological pH value in the spinal cord in rat is about 7.4 [31]. However, mild systemic acidosis could occur within hours after SCI and the pH value may decrease [32]. We injected the material 24 h after the injury, a time point by which the pH in the injured tissue has returned to normal physiological conditions [31]. We found that the QL6 injected directly to the injured spinal cord yielded positive neuroanatomic and neurophysiological results. We did not observe acute systemic or local toxicity effects, as shown by our results acquired 1 week after QL6 injection, suggesting that using SAP QL6 with intrinsic pH close to physiological values could yield excellent biocompatibility, which may be critical for providing a microenvironment for cell–scaffold interaction.

4.2. Effects of SAP in alleviating SCI pathology and its possible mechanisms

The current lack of effective therapeutic options for curing SCI is due to the complexity of the pathophysiological events that occur after this trauma. These unfavorable events include inflammation, cell death, demyelination, axonal degeneration, and the formation of cavities that are initially lined by reactive gliosis and, subsequently, by glial scars [33,34]. The present results show that SAP QL6 scaffolds serve as a bridge to prevent the collapse of adjacent tissue, and alleviate the pathology of secondary injury including reduced apoptosis, inflammation, glial scarring and subsequent cyst formation. The decreased apoptosis and astrogliosis are correlated with a higher degree of tissue preservation at the injury site, and functional recovery.

The precise mechanisms for the effects of SAP are not yet known but our in vitro study of QL6 SAP culture and some previous findings may shed light on the potential mechanisms. It has been shown that, in vitro, the outer scaffold formed by the SAP can inhibit the ingrowth of a variety of cell types, including fibroblasts, into the porous scaffold [35]. This may reduce inflammatory cell infiltration after SCI, in turn reducing astrogliosis. As observed in our study, QL6 can significantly suppress astrocytic differentiation of cultured NPCs. Therefore, it is hypothesized that the SAP scaffold may impede scarring and subsequent cyst formation by suppressing cellular ingrowth through the outer scaffold. Histological analysis of the spinal cord tissues showed the reparative processes fostered by the presence of SAP QL6-based scaffold in the lesion site.

Of note, SAP QL6 significantly increased the axonal density in the CST in regions rostral to the injury center. Counts of FG-labeled neurons in brainstem nuclei revealed a statistically significant improvement with QL6 treatment in axonal survival of rubrospinal and total brainstem neurons. The observed increase in axonal density may be attributed to enhanced axonal preservation and/or axonal sprouting, leading to the conclusion that the biocompatible scaffold could preserve or attract nerve fibers and potentially ameliorate the locomotor recovery of SCI. We propose the following two explanations for the axonal preservation and/or regeneration. First, our in vitro data show that QL6 can direct the differentiation of neural precursor cells into neurons. This result is in agreement with several previous studies in which nanofibers were found to promote outgrowth of processes from cultured neurons and suppress astrocytic differentiation of cultured neural stem cells [30,36,37]. It is possible that QL6 promotes an exaggerated effect on neurite production. Second, in fact, macrophage activity has been found to induce axonal retraction/die-back in the sensory axons [38], as has glial scarring [33]. In the injured brain, SAPs have been found to reduce the glial reaction and inflammation in the surrounding brain tissue [9]. Recently, it has been reported that nanofibers exhibited cytoprotective and anti-inflammatory properties in vitro and in vivo [39]. Therefore, it is possible that the effect of SAPs in preserving axons is via their capability to inhibit glial scar formation and reduce inflammation. Further studies are underway to clarify the cellular molecular mechanisms underlying the action of QL6.

4.3. Functional assessment of QL6 effects with electrophysiological and neurobehavioral tests

The use of SAP QL6 nanofiber scaffold remarkably promoted axonal preservation and/or sprouting as shown by tract tracing techniques. This could play a major role in modulating various neuronal activities, including the conjoint increase in conduction velocity and locomotion, since functional recovery can be significantly enhanced even if a small amount of normal tissue survives [40]. To test this hypothesis, we implemented in vivo and ex vivo electrophysiological experiments and behavioral assessment with BBB score, which provided a complementary strategy to monitor therapeutic interventions in this SCI research. To the best of our knowledge, systematic in vitro and in vivo electrophysiological investigation testing the effects of SAPs has been missing from the literature to date. SCI generally causes decreased amplitude in CAPs in white matter axons [22]. The mechanism behind this involves the reduced number of physically intact axons, reduced axonal excitability, channel density and activation. Our histological data indicate that more axons were preserved in the QL6-treated group, potentially explaining the larger-amplitude MEP and CAPs recorded from the treated cords.

Previous studies also show that the refractoriness of axons increases after SCI, behavior that is mainly related to the selective survival of smaller diameter axons [24]. Alternatively, it may be that SCI-induced demyelination causes low axonal membrane capacitance and impairs its fast depolarization and repolarization, thus causing increased refractoriness. Our data show refractoriness is decreased after QL6 injection. It is therefore interesting to evaluate the above two possibilities, in order to tease out the fundamental cellular mechanisms underlying nanomaterial treatment in chronic SCI.

SCI is associated with a decreased axonal response to high-frequency stimulation in the injured cords. This decreased capability of axons to propagate action potentials at high frequency is believed to be associated with reductions in the myelin sheath, which compromises the membrane capacitance needed for normal action potential propagation in the surviving myelinated axons [24]. The fact that QL6 can enhance high-frequency conduction indicates that the biomaterial may have certain beneficial effects in

preventing oligodendrocyte cell death and preservation of myelinated axons. It has been observed that self-assembly nanofibers could cause an increase in the number of oligodendrocytes in the injured spinal cord [7] and the increased number of oligodendrocytes at the site of injury could facilitate remyelination of axons that traverse the lesion [41,42]. Therefore, it is possible that QL6 will alleviate these impairments after SCI by enhancing remyelination to the spared, demyelinated axons around the epicenter.

5. Conclusions

In summary, the present study indicates that SAP QL6 nanofibers induced favorable reparative processes, and provides evidence that neural repair after SCI could be accomplished by the application of a synthetic, biocompatible, scaffolding material without including bioactive sequences in the SAP. Although the QL6 scaffold appears to play a significant role in functional recovery following SCI, one possible weakness of this biomaterial is the lack of neurons or neurofibers in the grafted scaffold [9,43]. In order to overcome this obstacle, we are investigating improved strategies to further utilize the features of this scaffold, such as using it in combination with neural stem cells or growth factors, for subacute and chronic SCIs in which repair is highly challenging. This combinatorial approach using SAP QL6 will be critical to achieve the greatest recovery, and may constitute a promising biocompatible scaffold approach for regenerative applications in the injured central nervous system. It is hoped this will eventually lead to the development of effective experimental therapies in humans.

Disclosure

The study was sponsored by Covidien who supplied the QL6 SAP.

Acknowledgements

The authors would like to thank Dr. Jeffrey D. Hartgerink for the preparation of the fluorescent tagged QL6 peptide, Jenny Oh for assistance with the histochemistry experiments, Behzad Azad for his help with behavioral testing, Jian Wang for help with cell culture, Giovanni Battista Calvieri and Steven Doyle for assistance with EM experiments and Madeleine O'Higgins for her editorial reviews. This study was supported by operating grant from Canadian Institutes of Health Research and the Gerry and Tootsie Halbert Chair in Neural Repair and Regeneration (held by Dr. Michael G. Fehlings).

Appendix A. Figures with essential colour discrimination

Certain figures in this article, particularly Figs. 1–6 and 9, are difficult to interpret in black and white. The full colour images can be found in the on-line version, at http://dx.doi.org/10.1016/j.actbio.2013.06.001.

References

[1] Fehlings MG, Tator CH, Linden RD. The relationships among the severity of spinal cord injury, motor and somatosensory evoked potentials and spinal cord blood flow. Electroencephalogr Clin Neurophysiol 1989;74:241–59.
[2] Thuret S, Moon LD, Gage FH. Therapeutic interventions after spinal cord injury. Nat Rev Neurosci 2006;7:628–43.
[3] Matson JB, Stupp SI. Self-assembling peptide scaffolds for regenerative medicine. Chem Commun (Camb) 2012;48:26–33.
[4] Holmes TC, de Lacalle S, Su X, Liu G, Rich A, Zhang S. Extensive neurite outgrowth and active synapse formation on self-assembling peptide scaffolds. Proc Natl Acad Sci USA 2000;97:6728–33.
[5] Zhang S. Designer self-assembling Peptide nanofiber scaffolds for study of 3-d cell biology and beyond. Adv Cancer Res 2008;99:335–62.
[6] Loo Y, Zhang S, Hauser CA. From short peptides to nanofibers to macromolecular assemblies in biomedicine. Biotechnol Adv 2012;30:593–603.
[7] Tysseling-Mattiace VM, Sahni V, Niece KL, Birch D, Czeisler C, Fehlings MG, et al. Self-assembling nanofibers inhibit glial scar formation and promote axon elongation after spinal cord injury. J Neurosci 2008;28:3814–23.
[8] Guo J, Su H, Zeng Y, Liang YX, Wong WM, Ellis-Behnke RG, et al. Reknitting the injured spinal cord by self-assembling peptide nanofiber scaffold. Nanomedicine 2007;3:311–21.
[9] Guo J, Leung KK, Su H, Yuan Q, Wang L, Chu TH, et al. Self-assembling peptide nanofiber scaffold promotes the reconstruction of acutely injured brain. Nanomedicine 2009;5:345–51.
[10] Cigognini D, Satta A, Colleoni B, Silva D, Donega M, Antonini S, et al. Evaluation of early and late effects into the acute spinal cord injury of an injectable functionalized self-assembling scaffold. PLoS ONE 2011;6:e19782.
[11] Dong H, Paramonov SE, Aulisa L, Bakota EL, Hartgerink JD. Self-assembly of multidomain peptides: balancing molecular frustration controls conformation and nanostructure. J Am Chem Soc 2007;129:12468–72.
[12] Fehlings MG, Tator CH. The relationships among the severity of spinal cord injury, residual neurological function, axon counts, and counts of retrogradely labeled neurons after experimental spinal cord injury. Exp Neurol 1995;132:220–8.
[13] Liu Y, Figley S, Spratt SK, Lee G, Ando D, Surosky R, et al. An engineered transcription factor which activates VEGF-A enhances recovery after spinal cord injury. Neurobiol Dis 2009;37:384–93.
[14] Gelain F, Panseri S, Antonini S, Cunha C, Donega M, Lowery J, et al. Transplantation of nanostructured composite scaffolds results in the regeneration of chronically injured spinal cords. ACS Nano 2011;5:227–36.
[15] Kanazawa H, Ohsawa K, Sasaki Y, Kohsaka S, Imai Y. Macrophage/microglia-specific protein Iba1 enhances membrane ruffling and Rac activation via phospholipase C-gamma-dependent pathway. J Biol Chem 2002;277:20026–32.
[16] Karimi-Abdolrezaee S, Eftekharpour E, Wang J, Schut D, Fehlings MG. Synergistic effects of transplanted adult neural stem/progenitor cells, chondroitinase, and growth factors promote functional repair and plasticity of the chronically injured spinal cord. J Neurosci 2010;30:1657–76.
[17] Agrawal SK, Fehlings MG. The effect of the sodium channel blocker QX-314 on recovery after acute spinal cord injury. J Neurotrauma 1997;14:81–8.
[18] Abercrombie M. Estimation of nuclear population from microtome sections. Anat Rec 1946;94:239–47.
[19] Rowland JW, Lee JJ, Salewski RP, Eftekharpour E, van der Kooy D, Fehlings MG. Generation of neural stem cells from embryonic stem cells using the default mechanism: in vitro and in vivo characterization. Stem Cells Dev 2011;20:1829–45.
[20] Fehlings MG, Nashmi R. A new model of acute compressive spinal cord injury in vitro. J Neurosci Methods 1997;71:215–24.
[21] Sinha K, Karimi-Abdolrezaee S, Velumian AA, Fehlings MG. Functional changes in genetically dysmyelinated spinal cord axons of shiverer mice: role of juxtaparanodal Kv1 family K+ channels. J Neurophysiol 2006;95:1683–95.
[22] Ye H, Buttigieg J, Wan Y, Wang J, Figley S, Fehlings MG. Expression and functional role of BK channels in chronically injured spinal cord white matter. Neurobiol Dis; 2012.
[23] Stys PK, Ransom BR, Waxman SG. Compound action potential of nerve recorded by suction electrode: a theoretical and experimental analysis. Brain Res 1991;546:18–32.
[24] Nashmi R, Fehlings MG. Changes in axonal physiology and morphology after chronic compressive injury of the rat thoracic spinal cord. Neuroscience 2001;104:235–51.
[25] Basso DM, Beattie MS, Bresnahan JC. A sensitive and reliable locomotor rating scale for open field testing in rats. J Neurotrauma 1995;12:1–21.
[26] Sofroniew MV. Molecular dissection of reactive astrogliosis and glial scar formation. Trends Neurosci 2009;32:638–47.
[27] Casha S, Yu WR, Fehlings MG. Oligodendroglial apoptosis occurs along degenerating axons and is associated with FAS and p75 expression following spinal cord injury in the rat. Neuroscience 2001;103:203–18.
[28] Eftekharpour E, Karimi-Abdolrezaee S, Sinha K, Velumian AA, Kwiecien JM, Fehlings MG. Structural and functional alterations of spinal cord axons in adult Long Evans Shaker (LES) dysmyelinated rats. Exp Neurol 2005;193:334–49.
[29] Vasita R, Katti DS. Nanofibers and their applications in tissue engineering. Int J Nanomedicine 2006;1:15–30.
[30] Silva GA, Czeisler C, Niece KL, Beniash E, Harrington DA, Kessler JA, et al. Selective differentiation of neural progenitor cells by high-epitope density nanofibers. Science 2004;303:1352–5.
[31] Huang PP, Young W. The effects of arterial blood gas values on lesion volumes in a graded rat spinal cord contusion model. J Neurotrauma 1994;11:547–62.
[32] Vink R, Noble LJ, Knoblach SM, Bendall MR, Faden AI. Metabolic changes in rabbit spinal cord after trauma: magnetic resonance spectroscopy studies. Ann Neurol 1989;25:26–31.
[33] Fitch MT, Silver J. CNS injury, glial scars, and inflammation: Inhibitory extracellular matrices and regeneration failure. Exp Neurol 2008;209:294–301.
[34] Baptiste DC, Fehlings MG. Update on the treatment of spinal cord injury. Prog Brain Res 2007;161:217–33.
[35] Teng YD, Lavik EB, Qu X, Park KI, Ourednik J, Zurakowski D, et al. Functional recovery following traumatic spinal cord injury mediated by a unique polymer scaffold seeded with neural stem cells. Proc Natl Acad Sci USA 2002;99:3024–9.

[36] Cunha C, Panseri S, Villa O, Silva D, Gelain F. 3D culture of adult mouse neural stem cells within functionalized self-assembling peptide scaffolds. Int J Nanomedicine 2011;6:943–55.
[37] Gelain F, Cigognini D, Caprini A, Silva D, Colleoni B, Donega M, et al. New bioactive motifs and their use in functionalized self-assembling peptides for NSC differentiation and neural tissue engineering. Nanoscale 2012;4:2946–57.
[38] Horn KP, Busch SA, Hawthorne AL, van Rooijen N, Silver J. Another barrier to regeneration in the CNS: activated macrophages induce extensive retraction of dystrophic axons through direct physical interactions. J Neurosci 2008;28:9330–41.
[39] Wang Y, Bakota E, Chang BH, Entman M, Hartgerink JD, Danesh FR. Peptide nanofibers preconditioned with stem cell secretome are renoprotective. J Am Soc Nephrol 2011;22:704–17.
[40] Beattie MS, Farooqui AA, Bresnahan JC. Review of current evidence for apoptosis after spinal cord injury. J Neurotrauma 2000;17:915–25.
[41] Keirstead HS, Blakemore WF. The role of oligodendrocytes and oligodendrocyte progenitors in CNS remyelination. Adv Exp Med Biol 1999;468:183–97.
[42] Karimi-Abdolrezaee S, Eftekharpour E, Wang J, Morshead CM, Fehlings MG. Delayed transplantation of adult neural precursor cells promotes remyelination and functional neurological recovery after spinal cord injury. J Neurosci 2006;26:3377–89.
[43] Zhang H, Hayashi T, Tsuru K, Deguchi K, Nagahara M, Hayakawa S, et al. Vascular endothelial growth factor promotes brain tissue regeneration with a novel biomaterial polydimethylsiloxane-tetraethoxysilane. Brain Res 2007;1132:29–35.